Materials Today Physics 13 (2020) 100215

Contents lists available at ScienceDirect

Materials Today Physics

journal homepage: https://www.journals.elsevier.com/materials-today-physics

Enhancing the figure of merit in thermoelectric materials by adding silicate aerogel

T.-W. Lan [a, 1], K.-H. Su [a, b, 1], C.-C. Chang [a, c, d], C.-L. Chen [a], C.-L. Chen [e], M.-N. Ou [a], D.-Z. Wu [a], P.M. Wu [a, f], C.-Y. Su [b], M.-K. Wu [a, *], Y.-Y. Chen [a, **]

[a] Institute of Physics, Academia Sinica, Taipei, 11529, Taiwan
[b] Institute of Mechatronic Engineering, National Taipei University of Technology, Taipei, 106, Taiwan
[c] Research Center of Digital Oral Science and Technology, College of Oral Medicine, Taipei Medical University, Taipei, 11031, Taiwan
[d] School of Dental Technology, College of Oral Medicine, Taipei Medical University, Taipei, 11031, Taiwan
[e] National Synchrotron Radiation Research Center, Hsinchu, 30076, Taiwan
[f] BitSmart LLC, San Mateo, CA 94403, USA

ARTICLE INFO

Article history:
Received 11 February 2020
Received in revised form
19 March 2020
Accepted 21 March 2020
Available online 2 April 2020

Keywords:
p-type $Bi_{0.5}Sb_{1.5}Te_3$
p-type MgAgSb
Phonon
Seebeck coefficient
Thermal conductivity

ABSTRACT

To achieve practical applications of thermoelectric materials in large scale, materials with high thermal conversion efficiency, low cost, and operating at a proper temperature range are required. Owing to the inversely relationship between electrical conductivity (σ) and Seebeck coefficient (S), it is a great challenge to improve high power factor ($PF = \sigma S^2$) of a thermoelectric material. Here, we show that by adding a small amount of silicate aerogel to existing promising materials, including $Bi_{0.5}Sb_{1.5}Te_3$ (*p*-type), $Cu_{0.01}Bi_2Te_{2.7}Se_{0.3}$ (*n*-type), and *p*-type MgAgSb, significantly improves the figure of merit (*zT*) of the materials. For the BiTe-based materials, the primary gain in *zT* comes from a significant reduced thermal conductivity, while preserving high PF for the aerogel mixed composites. On the other hand, the enhancement of *zT* in aerogel-added *p*-type $MgAg_{0.97}Sb_{0.99}$ material is not due to the reduction in thermal conductivity but rather an enhancement in PF, which is important for practical applications. Furthermore, the materials we present in this work are bulk polycrystalline samples, which are relatively easy to produce without complicated synthesis processes.

Thermoelectric materials offer a great potential for directly converting waste heat into electricity and are considered essential for renewable energy application. The challenge for practical applications of thermoelectric materials in large scale requires materials with high thermal conversion efficiency, low cost, and operating at a proper temperature range. The thermoelectric performance of material is assessed by the dimensionless figure of merit, $zT = S^2\sigma T/\kappa$, where *T*, *S*, σ, and κ are absolute temperature, Seebeck coefficient, electrical, and thermal conductivity, respectively [1]. Simultaneously attaining good electrical properties and minimizing thermal conductivity will lead to a high *zT* value. However, it has been a great challenge to improve the power factor ($PF = \sigma S$ [2]) of a thermoelectric material due to the inversely relationship between σ and *S*. Most of the remarkable enhancements of *zT* reported have largely relied on the reduction of thermal conductivity via increasing phonon scattering in material structures, such as dislocations, grain boundaries, interfaces, and precipitates [2–4].

Bi_2Te_3-based materials are currently the best thermoelectric materials near room temperature; however, their wide applications are limited by the low thermoelectric conversion efficiency [5,6]. On the other hand, a record high thermoelectric conversion efficiency of 8.5% based on the *p*-type MgAgSb-based compound operating between 20 and 245 °C has been experimentally demonstrated [7]. Similar efficiencies have only been demonstrated at twice the temperature difference with hot side temperatures beyond 500 °C. The demonstration of this record high conversion efficiency at a relatively low temperature difference of 225 °C is an important step toward large-scale applications of thermoelectric devices.

* Corresponding author.
** Corresponding author.
E-mail addresses: mkwu@phys.sinica.edu.tw (M.-K. Wu), cheny2@phys.sinica.edu.tw (Y.-Y. Chen).
[1] These authors contributed equally to this work.

https://doi.org/10.1016/j.mtphys.2020.100215

At present, most research efforts are mainly devoted to enhance the materials' *zT* values through banggap [8–12] or phonon engineering [13]. For example, an attractive idea to significantly reduce lattice thermal conductivity is to create dense dislocation arrays on the grain boundaries using a liquid-phase sintering technique [14]. However, the dense dislocation-generation approach requires efforts to ensure the reliability and reproducibility in the scale-up synthesis process. It is known that to improve the critical current density of a superconductor for practical applications, the best approach is to introduce controllable defects to improve the flux pinning without affecting the characteristics of the superconducting matrix [15].

Following the same idea, we describe in this article the synthesis and characterizations of silicate aerogel-incorporated *p*-type $Bi_{0.5}Sb_{1.5}Te_3$ (BST), *n*-type $Cu_{0.01}Bi_2Te_{2.7}Se_{0.3}$ (BTS), and *p*-type $MgAg_{0.97}Sb_{0.99}$ (*p*-MAS) composites. We choose this particular MAS composition as it has been shown to exhibit much better thermoelectric performance than that of the stoichiometric material [16]. By mixing aerogel with a thermoelectric material, we expect the aerogel to serve as the key medium to reduce thermal conductivity, while preserving the PF so that overall enhancement in *zT* value can be achieved. We find that the silicate aerogel not only effectively suppresses the phonon propagation but also selectively scatters carriers within samples. Consequently, the *zT* enhancement by ~30% in both *p*-type BST and *n*-type BTS aerogel composites and a maximum of ~40% *zT* improvement in *p*-MAS are achieved. In addition, the polycrystalline nature of the composites makes the preparation of the final products relatively easy without complicated processes. Thus, the aerogel incorporation presented in this work could be an effective way to boost the practical application of thermoelectric materials.

1. Materials and methods

We used the conventional processes to prepare *p*-type Bi0.5Sb1.5Te3 (*p*-BST) and *n*-type $Cu_{0.01}Bi_2Te_{2.7}Se_{0.3}$ (*n*-BTS) materials using high purity Bi, Sb, Te, Se, and Cu elements. Ternary *p*-type $MgAg_{0.97}Sb_{0.99}$ (*p*-MAS) samples were prepared by solid-state synthesis with ball milling and hot pressing. The obtained ingots were ground into fine powders and further mixed with the hydrophilic silicate aerogel (Figs. S1 and 2). There are two types of aerogel, one is low-density (LD) aerogel, with a mass density of ~1 mg/cm3, and the other is high-density (HD) aerogel, with a mass density of ~10 mg/cm3. The differences between them are the number and size of porosity.[17] We found that both HD and LD aerogels have similar effects on the thermoelectric properties of both *p*-type (BST) and *n*-type (BTS) materials. And we have also tested with different aerogel concentrations. The data show consistently that the best results are with 0.67 wt% aerogel added to both *p*-BST and *n*-BTS materials, whereas for (α-MAS) material 0.3 wt% added aerogel gives the best result.

The mixed powders were pressed using the spark plasma sintering (SPS, SPS-515S, SYNTEX INC) at 673 K and 50 MPa under vacuum for 5 min to form a dense pellet. The structural phase, chemical compositions, and microstructures of samples were examined by powder x-ray diffraction (XRD, PANalytical X'Pert Pro) and scanning electron microscopy (SEM JXA-8200, JEOL). The measurements of electrical resistivity and Seebeck coefficient were carried out by the commercial system (ZEM-3, ULVAC-RIKO). The values of thermal conductivity were determined using the equation $\kappa = \lambda D C_p$, where λ, *D*, and C_p are the thermal diffusivity, mass density, and specific heat, respectively. The thermal diffusivity was measured by the laser flash method (LFA-457, NETZSCH), and the specific heat was measured using a differential scanning calorimeter (DSC-Q100, TA). The mass density was calculated using the Archimedes method. The Hall measurements were performed in a physical property measurement system (Quantum Design). X-ray absorption near-edge spectrum was performed at the Synchrotron Radiation Research Center in Taiwan. The monochromator Si (111) crystals were used in beamline 17C and 01C with a resolving power E/ΔE of better than 7000. A piece of metal foil was used for energy calibration.

1.1. Results on p-type and n-type BiTe-based materials

The XRD patterns of *p*-type, *n*-type materials, and the aerogel-added BiTe-based specimens are presented in Fig. 1(a) and (b). All the samples show the characteristic diffraction peaks from the Bi0.5Sb1.5Te3 and $Cu_{0.01}Bi_2Te_{2.7}Se_{0.3}$ rhombohedral phase, without noticeable impurity peaks. There is no obvious change in diffraction peak with adding silicate aerogels, thus the incorporation of aerogel to the matrix does not change the crystal structures of *p*-BST and *n*-BTS. The detailed XRD analysis on p-BST with different aerogel concentrations and the distribution of chemical composition in aerogel-added sample are presented in Figs. S3–5.

Fig. 2 shows the temperature dependence of thermoelectric properties for *p*-BST and *n*-BTS samples. All samples show that the electrical resistivity increases monotonically with temperature, indicating a typical degenerate semiconductor behavior. Compared with the pristine *p*-BST, there are ~15% decrease in resistivity at 400 K by adding 0.67 wt % silicate aerogel [Fig. 2(a)]. On the other hand, however, addition of 0.67 wt % aerogel increases ~20% resistivity for *n*-type BTS materials in comparison with the pristine sample. [Fig. 2(a)].

The temperature dependence of Seebeck coefficients for both *p*-type and *n*-type specimens are shown in Fig. 2(b). For 0.67 wt % aerogel *p*-type BST, the Seebeck coefficient decreases with aerogel addition, showing a similar trend of aerogel content–dependent electrical resistivity, that is, lower resistivity and lower Seebeck coefficient indicate hole carrier concentration increase after aerogel adding. However, the calculated PF of 0.67 wt % aerogel *p*-type BST at 300 K is ~4000 μW/m-K2 and is almost the same as the value of pristine BST. It is noted that the PF for aerogel-added sample remains about the same as the pristine material over the entire measured temperature range (Fig. S6).

The temperature dependence of the total thermal conductivity κ_{tot} is shown in Fig. 2(c). A remarkable reduction ~21% at 360 K of total thermal conductivity was observed in the 0.67 wt % aerogel-added *p*-BST. It is known that the total thermal conductivity κ_{tot} is the sum of the electronic contribution κ_{carr} and the lattice contribution κ_L [17,18]. The κ_L can be calculated from κ_{tot} by subtracting $\kappa_{carr,}$ and thus the κ_{carr} and κ_L versus temperature for all samples are obtained (Fig. S7). It is noticed the aerogel addition to the pristine BST can significantly reduce the thermal conductivity of lattice phonons about 30% over the whole temperature range. The total thermal conductivity exhibits a minimum ~0.8 W/m-K at ~350 K for the aerogel-added specimens. This thermal conductivity minimum seems to limit lower bound with increasing aerogel content.

It has been experimentally observed that the low-energy grain boundaries in *p*-BST are likely formed when atomic displacements are primarily in the Te–Te van der Waals layer. Displacements in this layer are likely to be least disruptive to the charge carriers and maintain high mobility. Most likely the added aerogel particles are randomly connected to these low-energy grain boundaries. Therefore, the grain boundaries with silicate-aerogel do maintain high charge-carrier mobility but provide sufficient atomic strain to scatter heat-carrying phonons. In addition, the microstructure of the aerogel-added sample was investigated by high-resolution transmission electron microscopy (HRTEM). From the HRTEM

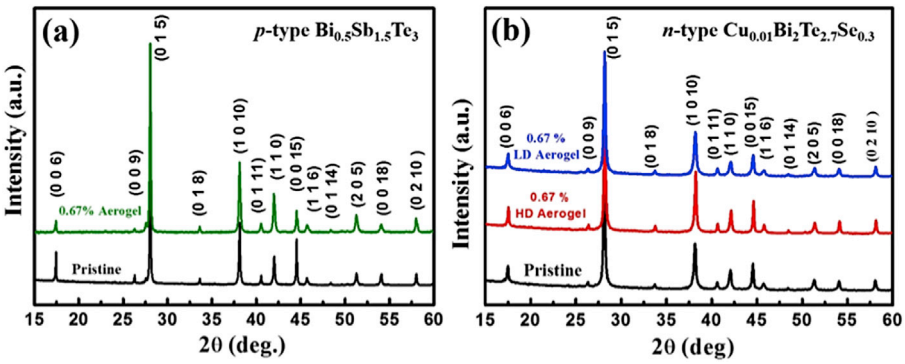

Fig. 1. (a) XRD patterns of pristine BST and BST mixed with 0.67% silicate aerogel samples, (b) XRD patterns of pristine BTS and BTS mixed with 0.67% HD and LD silicate aerogel samples. XRD, x-ray diffraction; BTS, $Bi_2Te_{2.7}Se_{0.3}$; BST, $Bi_{0.5}Sb_{1.5}Te_3$; HD, high-density; LD, low-density.

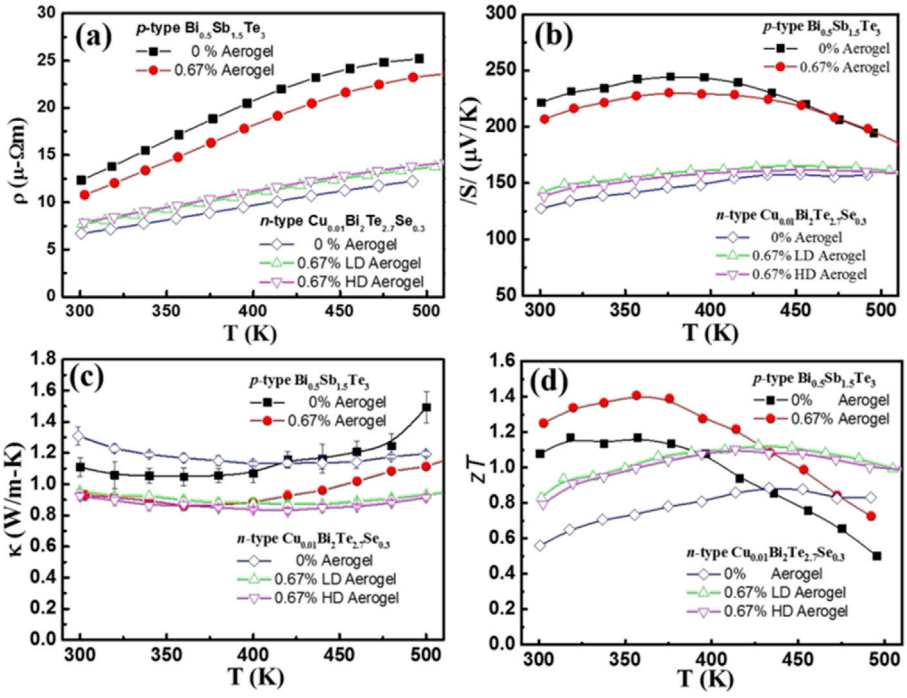

Fig. 2. Temperature dependence of electrical resistivity (a), Seebeck coefficients (b), thermal conductivity (c) and *zT* (d) for *p*-type BST and *n*-type BTS samples with different silicate aerogel contents. BTS, $Bi_2Te_{2.7}Se_{0.3}$; BST, $Bi_{0.5}Sb_{1.5}Te_3$; *zT, figure of merit.*

images, we can understand that the significant thermal conductivity reduction was attributed to the collective strong phonon scattering by interfaces in the nanostructures, containing aerogel-introduced strained boundaries, amorphous/crystalline interfaces, strains, planar defects, and mesoscale boundaries (Fig. 3).

The temperature dependence of *zT* for 0.67 wt% aerogel added *p*-BST is shown in Fig. 2(d). The incorporation of aerogel in the BST matrix distinctly boosts *zT* to a peak value of ~1.45 at 350 K. Because the Seebeck coefficient of aerogel addition specimens does not show an obvious increase, the significant *zT* enhancement is attributed to the increased electrical/thermal conductivity ratio (σ/κ). A high σ/κ ratio usually indicates excellent decoupling of phonon and carrier transport within the material.[19] When adding aerogel to the BST matrix, the σ/κ ratio is shown to increase substantially, with the largest increases more than 40% at 300−350 K (Fig. S8).

On the other hand, for *n*-type BTS materials, with 0.67 wt % aerogel-added sample, the increase in both Seebeck coefficient (~8%) and resistivity (~20%) shows the carrier concentration decrease [Fig. 2(b)]. The resistivity and Seebeck coefficient trend change in the *n*- and *p*-type aerogel samples suggest that the hole carriers increase in both types by the addition of silicate aerogel, indicating Si might get in the lattice or change the dangling bonds at grains boundary. Overall, a comparable high PF of ~2550 μW/m-K2 at 350 K is obtained for 0.67 wt% aerogel-added *n*-BTS (Figs. S12 and 13). Similar to the *p*-type BST, the thermal conductivities of aerogel-added *n*-BTS dramatically decreased ~30% over the whole temperature range [Fig. 2(c)]. Consequently, the aerogel-added *n*-BTS exhibits a *zT* value ~1 at 350 K and even reaches a peak value of $zT = 1.12$ at 425 K [Fig. 2(d)].

To better understand the underlying mechanism for the observed sample, which preferentially scatters *n*-type carriers in aerogel-added samples, we used X-ray absorption near-edge spectroscopy to study the local electronic structure and chemical information [20]. Fig. 4(a) and (b) display the normalized Se K-edge ($1s \rightarrow 4sp$) and Te K-edge ($1s \rightarrow 5sp$) of X-ray absorption

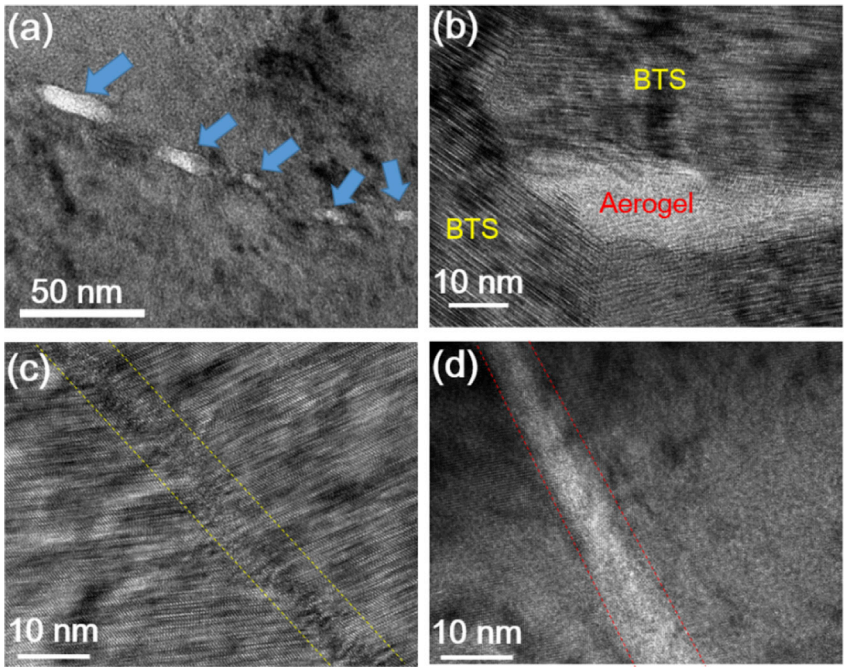

Fig. 3. (a) Bright field transmission electron microscopy (TEM) images of BTS/aerogel composite: the white blocks are corresponding to aerogels. (b) HRTEM image of aerogel embedded within the grains. (c) Formation of aerogel-introduced strain boundary. (d) High magnification image showing the interface between aerogel and BTS crystal grains. BTS, $Bi_2Te_{2.7}Se_{0.3}$.

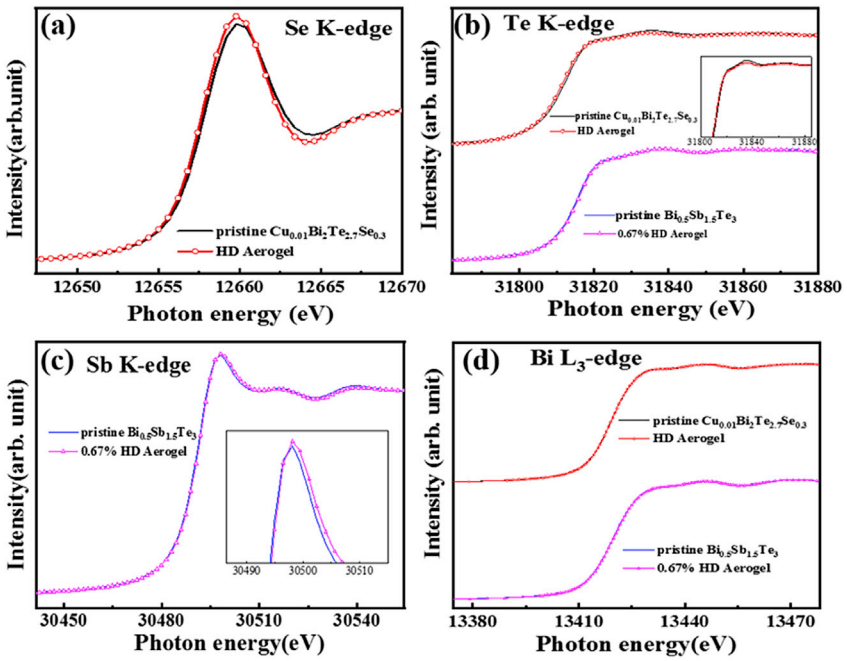

Fig. 4. X-ray absorption near-edge spectra of Se K-edge (a), Te K-edge (b), Sb K-edge (c) and Bi L3-edge (d) for the pristine and aerogel incorporated *n*-type BTS and p-type BST samples. BTS, $Bi_2Te_{2.7}Se_{0.3}$; BST, $Bi_{0.5}Sb_{1.5}Te_3$.

near edge structure (XANES) spectra of aerogel incorporated *n*-type BTS specimens at 300 K. They are mostly related to the partial density of states above the Fermi level of Se 4*p* and Te 5*p* unoccupied states. It is clear that the increased Se 4*p* peak intensity and slightly change of spectral line shape is when the aerogel is added, suggesting the occurrence of more Se 4*p* unoccupied state (hole carriers) with a distorted structural symmetry in Se ions environment, that is, a part of Se ions are replacing Te ions. Fig. 4(b) shows that the Te 5*p* peak intensity apparently decreased in aerogel addition specimen that is totally opposite to the spectra change of observation in Se K-edge [Fig. 4(a)]. These results imply that the Se 4*p* orbital loses charges and Te 5*p* orbital gains charges as aerogel is added. The slightly distorted lattice symmetry and electron charge transfer from Se 4*p* to Te 5*p* states become significant for the aerogel incorporated *n*-type BTS sample.

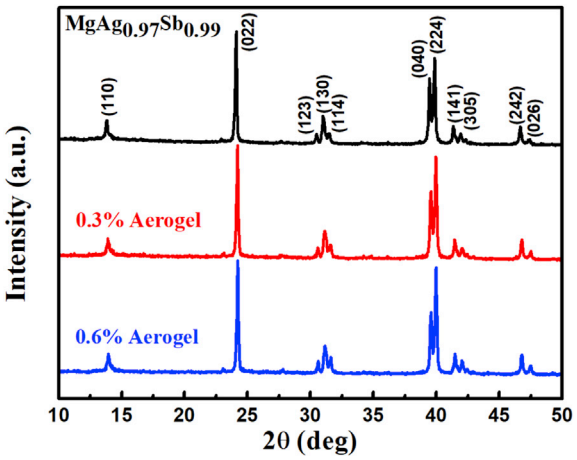

Fig. 5. Powder XRD diffraction patterns of pristine MAS and with 0.3 wt% and 0.6 wt% aerogel-added samples. XRD, x-ray diffraction; MAS, $MgAg_{0.97}Sb_{0.99}$.

Fig. 4(c) presents the normalized Sb K-edge ($1s \rightarrow 5sp$) XANES spectra of the pristine and 0.67 wt % aerogel-added *p*-type BTS measured at 300 K. A peak broadening feature and a chemical shift are observed in the high energy region around 30500 eV for the aerogel incorporated *p*-type BST sample. The local structural symmetry with distorted Sb—Te bond is appraised. These results are consistent with the enhancing lattice phonon scattering of aerogel addition for aerogel-added *n*-type and *p*-type specimens. Fig. 4(d) shows XANES Bi L_3-edge spectra of pristine and aerogel-added *p*-type and *n*-type specimens. These spectra show no detectable change in almost identical line shapes. The lattice structure distortion would highly correlate to the change of lattice phonons by replacing the cation (*p*-type) and anion (*n*-type).

1.2. Results on p-MAS

The preparation method of aerogel-added *p*-MAS is in accordance with the preparation method of the aforementioned BST/BTS composites. The detailed steps are summarized in Figs. S14–16. The XRD patterns of pristine and aerogel-added *p*-MAS are shown in Fig. 5. These diffraction patterns can all be well refined by the α-phase (tetragonal structure) with space group *I*4c2. The *a*-axis lattice constant of MAS increases from 9.167 Å to 9.1731 Å after 0.6 wt% aerogel doping. Meanwhile, the *c*-axis lattice constant also expands from 12.7190 Å to 12.7254 Å. The XRD results also confirm that the added-aerogel sample does intermix with the matrix MAS.

Fig. 6 shows the results of the thermal transport measurements on the studied *p*-MAS system. The temperature dependent resistivity of the pristine MAS sample follows the reported behavior [16], which shows a resistive maximum of ~37.8 μΩ-m at 360 K. The aerogel-added samples show substantial decrease in resistivity, at temperatures above 350 K, with the maximum reduction ~10% in 0.3 wt% aerogel-added sample. Nevertheless, with aerogel content up to 0.6 wt%, the resistivity values over the temperature range of interest are still close to 2% smaller than that of the pristine material.

Consistent with the results reported by Zhao et al. [16], we also observed all investigated samples exhibiting semiconductor-like behavior at temperature between 360 K and 560 K. We estimated the bandgap increasing from 0.129 eV for pristine sample to 0.294 eV for 0.3 wt% and 0.341 eV for 0.6 wt% aerogel-added

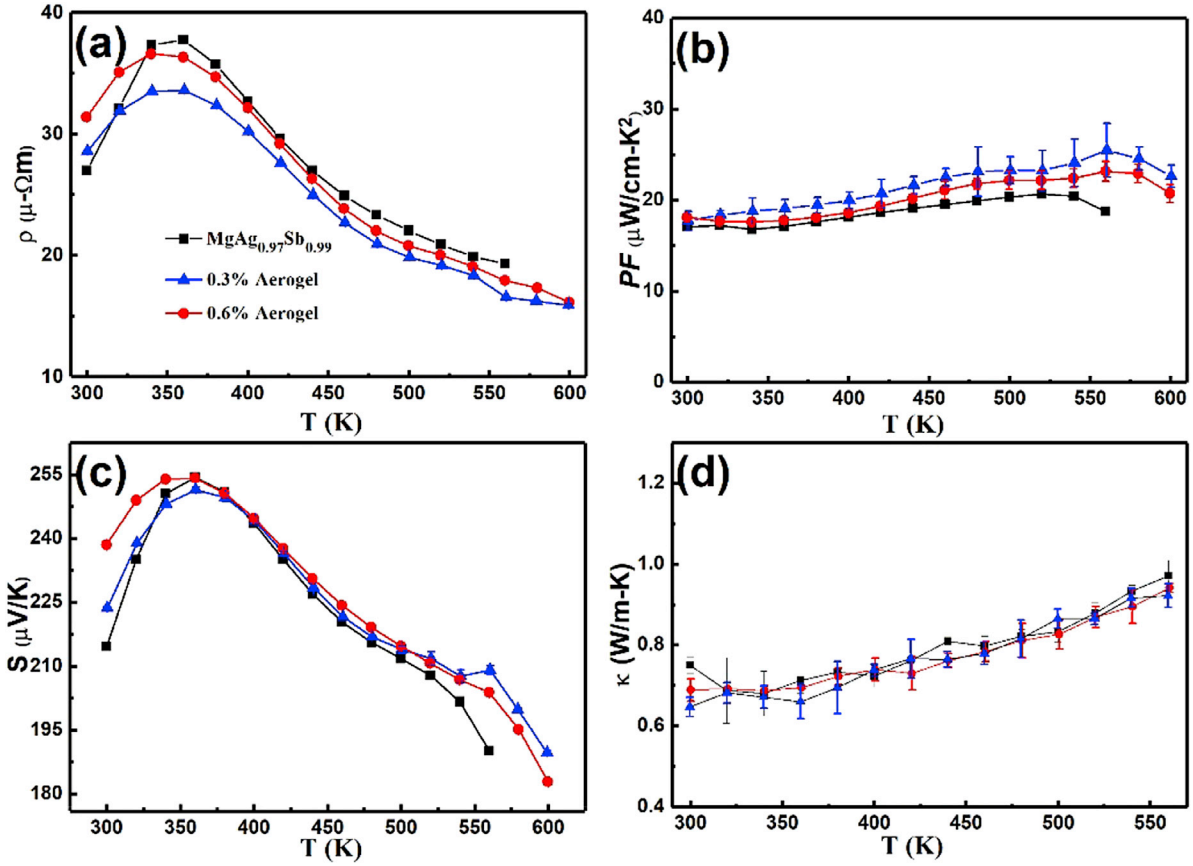

Fig. 6. Temperature dependent (a) electrical resistivity, (b) Seebeck coefficient, (c) power factor, and (d) thermal conductivity of MAS and aerogel-added samples. MAS, $MgAg_{0.97}Sb_{0.99}$.

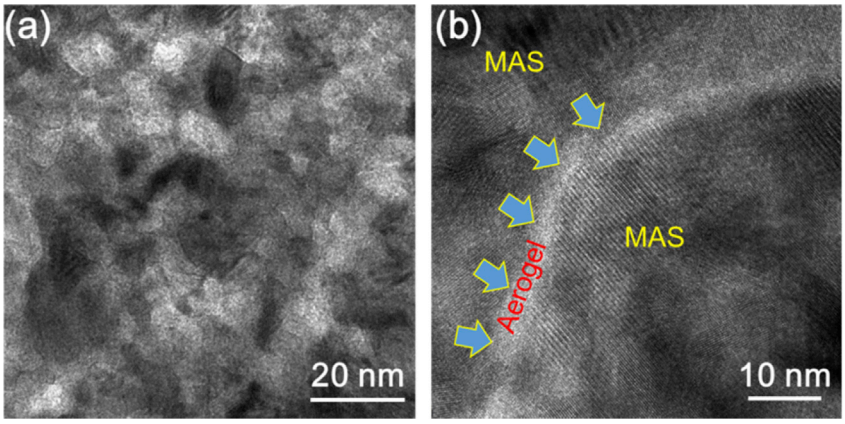

Fig. 7. Bright-field TEM images of MAS doped with 0.6% aerogel: (a) the distribution of aerogel particles (white blocks) in the MAS matrix, (b) HRTEM image reveals the existence of the MAS/aerogel boundary layer. MAS, $MgAg_{0.97}Sb_{0.99}$.

samples, even though the aerogel-added samples have lower overall resistivities (Fig. S17). This observation suggests that the added aerogel might not affect much the Seebeck coefficient at the temperature range of interest. Indeed, the temperature dependence Seebeck coefficient, as shown in Fig. 6(c), demonstrates these samples are *p*-type, and the values for all three samples are comparable and even become higher for aerogel-added samples at high temperature.

It was known [21] that the thermal expansion of the room temperature α phase becomes non-linear above 300 °C, which causes the sudden increase in conductivity and decrease in Seebeck coefficient. It was argued that these changes were due to the increasing tetragonal distortion as the phase approaches the transformation to the more anisotropic β phase, which remains to be tetragonal, that appears at ~330 °C. Thus, in the pristine sample, we did observe a slight drop in both resistivity and Seebeck coefficient. It is interesting to note that in the aerogel-added samples, the resistivity indeed decreases with even larger percentage. However, the Seebeck coefficient in fact increases slightly instead of decreasing. The combined effect will be to enhance the PF of MAS by adding aerogel. These observations suggest that the added aerogel may provide a mechanism to pin the tetragonal distortion of the matrix.

Fig. 6(b) plots the PF of the studied MAS materials. It clearly shows the improvement in PF above 320 K in both the aerogel-added samples with the 0.3 wt% added showing the highest PF, reaching 28.45 μW/cm-K [2] at 560 K, which has ~ 54% enhancement comparing with the pristine material at the same temperature. On the other hand, it is to our surprise that we do not observe distinguishable change in thermal conductivity, as shown in Fig. 6(d), by adding aerogel. Although the addition of aerogel to the MAS material will result in an increase in electrical conductivity and an increase in carrier thermal conductivity, the total thermal conductivity of the MAS material has not increased significantly as a result. After analyzing the carrier and lattice thermal conductivity, it can be found that the lattice thermal conductivity will be obviously reduced due to the addition of the aerogel (Fig. S18). The HRTEM observation reveals that the main reason may be that aerogels can create a lot of special amorphous/crystalline interface microstructures in the material, which will lead to a strong phonon scattering (Fig. 7).

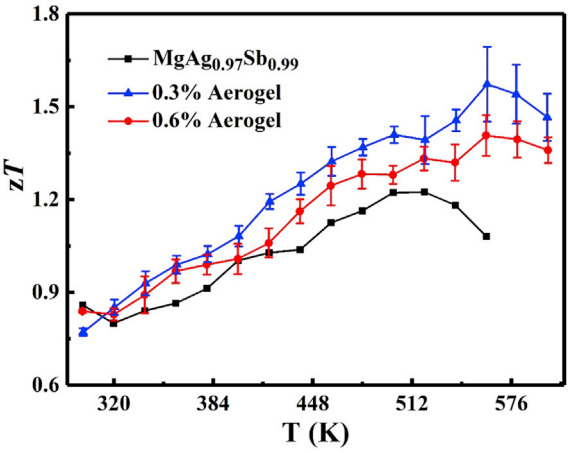

Fig. 8. Temperature-dependent zT for MAS and intercalated with aerogel-added samples. MAS, $MgAg_{0.97}Sb_{0.99}$; zT, figure of merit.

Fig. 8 displays the calculated figure of *zT* for pure MAS and aerogel-added MAS samples. Comparing with the maximum *zT* value of 1.22 of pure MAS at 500 K, both aerogel doped samples demonstrate higher *zT* at the same temperature. A more significantly enhancement was observed at ~550 K with *zT* value of 1.69 for 0.3 wt%. and 1.47 for 0.6 wt% doped MAS, respectively. Comparing with the pristine sample at the same temperature of 550 K, the enhancement in *zT* value is close to 54% for 0.3 wt% and 36% for 0.62wt% samples. Clearly, the enhancement in *zT* originates from the enhancement of PF by adding limited amount of aerogel. Adding more aerogel, in fact, does not further improve the thermoelectric performance of *p*-MAS. Our observations strongly suggest adding small amount of silicate aerogel to *p*-MAS may further improve its value for practical applications. It will be an interesting follow-up work using the aerogel-added *p*-MAS to check whether its energy conversion efficiency would be further enhanced.

2. Conclusion

In summary, we have demonstrated using aerogel addition to enhance the *zT* of the two most commonly used *n*- and *p*-type thermoelectric materials to record high levels. A record high *zT* ~1.45 at 350 K for *p*-type Bi0.5Sb1.5Te3 and *zT* ~1.12 at 425 K for *n*-type $Cu_{0.01}Bi_2Te_{2.7}Se_{0.3}$ were achieved. The primary gain in *zT* comes from a significant reduced thermal conductivity, while preserving high power factor for the aerogel mixed composites. We have also demonstrated the enhancement of the *zT* in aerogel-added *p*-type $MgAg_{0.97}Sb_{0.99}$ material with *zT* value of 1.69 for 0.3 wt% aerogel content at ~550 K. The mechanism in the case of MAS is not due to the reduction of thermal conductivity but rather the large enhancement in power factor, which is more important

for practical applications. Furthermore, the materials we present in this work are bulk polycrystalline samples, which make them more valuable due to the less complicated synthesis processes.

Author contributions

T.W.L. and K.H.S. contribute equally to this work, both carry out most of the material preparation, property characterizations, and data analysis and prepared the first draft of the article. C.C.C. and D.Z.W. contribute in material preparation, parts of X-ray diffraction work, and SEM observations. C.L.C. is responsible for detailed TEM observations and data analysis. M.N.O. is responsible for material processing and property characterizations. C.L.C. carried out the x-ray absorption experiment and analyzed the results. C.Y.S. contributes in data collection and analysis and Y.Y.C. is in charge of the overall experimental set-up and performance. P.M.W. and M.K.W. conceived the experiment, oversaw the experiments, and finalized the article. All authors have contributed to the final draft of the article.

Declaration of interests

The authors declare that they have no known competing financial interests or personal relationships that could have appeared to influence the work reported in this article.

Acknowledgments

The authors thank Dr. James Oyang of Pharos Science and Application Inc. for introducing to us the silicate aerogel and Dr. Peter Tsou of Jet Propulsion Laboratory (JPL) for supplying us the silicate-aerogel used in this study. We also appreciate the contribution from Mr. Ting Yi, who helped the preparation of the samples in this study. This work is financially supported by Ministry of Science and Technology (MOST), Taiwan, Grant No. MOST 106-2112-M-001-019-MY3 and the Academia Sinica research grant.

Appendix A. Supplementary data

Supplementary data to this article can be found online at https://doi.org/10.1016/j.mtphys.2020.100215.

References

[1] D.M. Rowe, Thermoelectrics Handbook: Macro to Nano, CRC press, 2005.
[2] K. Biswas, J. He, I.D. Blum, C.-I.I. Wu, T.P. Hogan, D.N. Seidman, V.P. Dravid, M.G. Kanatzidis, Nature 489 (2012) 414.
[3] K. Biswas, J. He, Q. Zhang, G. Wang, C. Uher, V.P. Dravid, M.G. Kanatzidis, Nat. Chem. 3 (2011) 160.
[4] J. He, S.N. Girard, M.G. Kanatzidis, V.P. Dravid, Adv. Funct. Mater. 20 (2010) 764.
[5] L.E. Bell, Science 321 (2008) 1457.
[6] W. Liu, J. Hu, S. Zhang, M. Deng, C.-G. Han, Y. Liu, Mater. Today Phys. 1 (2017) 50.
[7] D. Kraemer, J. Sui, K. McEnaney, H. Zhao, Q. Jie, Z.F. Ren, G. Chen, Energy Environ. Sci. 8 (2015) 1299.
[8] J.R. Sootsman, D.Y. Chung, M.G. Kanatzidis, Angew. Chem. Int. Ed. 48 (2009) 8616–8639.
[9] M.S. Dresselhaus, G. Chen, M.Y. Tang, R.G. Yang, H. Lee, D.Z. Wang, Z.F. Ren, J.-P. Fleurial, P. Gogna, Adv. Mater. 19 (2007) 1043–1053.
[10] G.J. Snyder, E.S. Toberer, Nat. Mater. 7 (2008) 105–114.
[11] M. Zebarjadi, K. Esfarjani, M.S. Dresselhaus, Z.F. Ren, G. Chen, Energy Environ. Sci. 5 (2012) 5147–5162.
[12] D. Kraemer, B. Poudel, H.-P. Feng, J.C. Caylor, B. Yu, X. Yan, Y. Ma, X. Wang, D. Wang, A.J. Muto, K. McEnaney, M. Chiesa, Z.F. Ren, G. Chen, Nat. Mater. 10 (2011) 532–538.
[13] Z. Chen, X. Zhang, Y. Pei, Adv. Mater. 30 (2018) 1705617.
[14] S.I. Kim, K.H. Lee, H.A. Mun, H.S. Kim, S.W. Hwang, J.W. Roh, D.J. Yang, W.H. Shin, X.S. Li, Y.H. Lee, G.J. Snyder, S.W. Kim, Science 348 (2015) 109.
[15] N. Kumar Sudesh, S. Das, C. Bernhard, G.D. Varma, Supercond. Sci. Technol. 26 (2013): 095008.
[16] H. Zhao, J. Sui, Z. Tang, Y. Lan, Q. Jie, D. Kraemer, K. McEnaney, A. Guloy, G. Chen, Z.F. Ren, Nano Energy 7 (2014) 97–103.
[17] M. Ashida, T. Hamachiyo, K. Hasezaki, H. Matsunoshita, M. Kai, Z. Horita, J. Phys. Chem. Solid. 70 (2009) 1089.
[18] R.J. Mehta, Y. Zhang, C. Karthik, B. Singh, R.W. Siegel, T.B. Tasciuc, G. Ramanath, Nat. Mater. 11 (2012) 233.
[19] W.T. Chiu, C.L. Chen, Y.Y. Chen, Sci. Rep. 6 (2016) 23143.
[20] C.C. Hsu, C.W. Pao, J.L. Chen, C.L. Chen, C.L. Dong, Y.S. Liu, J.F. Lee, T.S. Chan, C.L. Chang, Y.K. Kuo, C.S. Lue, Europhys. Lett. 106 (2014) 37007.
[21] M.J. Kirkham, A.M. dos Santos, C.J. Rawn, E. Lara-Curzio, J.W. Sharp, A.J. Thompson, Phys. Rev. B85 (2012) 144120.